Matter and Radiation at Extremes

RESEARCH ARTICLE

pubs.aip.org/aip/mre

The effects of incident light wavelength difference on the collective stimulated Brillouin scattering in plasmas

Cite as: Matter Radiat. Extremes 8, 055602 (2023); doi: 10.1063/5.0151372
Submitted: 21 March 2023 • Accepted: 9 July 2023 •
Published Online: 28 July 2023

Qiang Wang,[1] Zhichao Li,[2] Zhanjun Liu,[1,3,a)] Tao Gong,[2] Wenshuai Zhang,[1] Tao Xu,[2] Bin Li,[1] Ping Li,[2] Xin Li,[1] Chunyang Zheng,[1,3] Lihua Cao,[1,3] Xincheng Liu,[2] Kaiqiang Pan,[2] Hang Zhao,[2] Yonggang Liu,[2] Bo Deng,[2] Lifei Hou,[2] Yingjie Li,[2] Xiangming Liu,[2] Yulong Li,[2] Xiaoshi Peng,[2] Zanyang Guan,[2] Qiangqiang Wang,[2] Xingsen Che,[2] Sanwei Li,[2] Qiang Yin,[2] Wei Zhang,[2] Liqiong Xia,[2] Peng Wang,[2] Xiaohua Jiang,[2] Liang Guo,[2] Qi Li,[2] Minqing He,[1] Liang Hao,[1] Hongbo Cai,[1,3] Wudi Zheng,[1] Shiyang Zou,[1] Dong Yang,[2] Feng Wang,[2] Jiamin Yang,[2] Baohan Zhang,[2] Yongkun Ding,[1,3] and Xiantu He[1,3]

AFFILIATIONS

[1] Institute of Applied Physics and Computational Mathematics, Beijing 100094, China
[2] Laser Fusion Research Center, China Academy of Engineering Physics, Mianyang, Sichuan 621900, China
[3] HEDPS, Center for Applied Physics and Technology, and College of Engineering, Peking University, Beijing 100871, China

[a)] **Author to whom correspondence should be addressed:** liuzj@iapcm.ac.cn

ABSTRACT

The first laser–plasma interaction experiment using lasers of eight beams grouped into one octad has been conducted on the Shenguang Octopus facility. Although each beam intensity is below its individual threshold for stimulated Brillouin backscattering (SBS), collective behaviors are excited to enhance the octad SBS. In particular, when two-color/cone lasers with wavelength separation 0.3 nm are used, the backward SBS reflectivities show novel behavior in which beams of longer wavelength achieve higher SBS gain. This property of SBS can be attributed to the rotation of the wave vectors of common ion acoustic waves due to the competition of detunings between geometrical angle and wavelength separation. This mechanism is confirmed using massively parallel supercomputer simulations with the three-dimensional laser–plasma interaction code LAP3D.

I. INTRODUCTION

In laser indirect drive inertial confinement fusion (ICF) experiments, laser energy that has survived backscattering and inverse-bremsstrahlung damping along the journey through plasmas formed from filler gas and ablated hohlraum wall is converted to x rays in the high-atomic-number plasmas near the critical density, and it then drives the fuel capsule.[1–3] The backscattering consists mainly of laser–plasma instabilities (LPIs), such as stimulated Brillouin backscattering (SBS) and stimulated Raman scattering (SRS). LPIs may cause significant energy loss, impacting the symmetry and efficiency of the implosion of the capsule. To improve the achievable nuclear fusion gain, it is therefore crucially important to understand and control LPIs. Since energies as high as the megajoule range, as well as hundreds of beams, are needed, a strategy is usually adopted in which several beams are bundled together and injected into the target chamber through a single common port. Forming very small angles, these beams nearly completely overlap each other in the hohlraum plasma, in contrast to the case of a single beam or the widely studied scheme in which cross-beam energy transfer (CBET) occurs between multiple beams.[4–8] Besides their relevance to ICF, interactions of multiple beams in a plasma have also attracted much attention in the context of plasma optics owing to the possibility of raising the damage thresholds of intensity and fluence compared with those in solid optics.[9,10]

Symmetrically localized beams in a cone with equal intensity may excite a collective mode: either a shared plasma wave (SP) mode, in which a common plasma wave [ion acoustic wave (IAW) or electron plasma wave (EPW)] is driven along the symmetry axis, or a shared scattering light wave (SL) mode, in which a common backscattered light wave is driven along the symmetry axis. These modes have been experimentally observed in SBS and SRS.[11–14] With multiple beams, the thresholds for these collective instabilities may be exceeded even when the intensities of the individual beams are below the thresholds for single-beam instabilities.[15,16] With their mutual enhancement, in the case of maximum coupling, the gain of the collective instabilities increases in proportion to the number of beams, N. Theoretically, SBS with SP mode has a lower threshold and higher growth rate than SBS with SL mode.[16] Therefore, understanding of such collective effects is of great relevance to ICF experiments.

To mitigate LPI, from the laser side, early theoretical and experimental studies showed that the use of broadband lasers could reduce the temporal growth rate.[17–21] Recently, multiple-beam broadband lasers have been investigated with the aim of lowering the thresholds for absolute SRS and two-plasmon decay instabilities.[22] In this work, we report the results of experimental studies and numerical simulations of collective SBS driven by two-color/cone eight-beam lasers on the Shenguang Octopus facility. A novel modulation of SBS by small-wavelength shift is found and is explained both theoretically and numerically.

II. EXPERIMENTAL SETUP AND RESULTS

Recently, a new laser facility named Shenguang Octopus has been constructed to study the LPIs excited by bundled multiple beams and to optimize beam smoothing techniques. Figure 1 shows a schematic of the octad on the Shenguang Octopus. Eight laser beams are bundled together and directed into a cylindrical target.[23,24] These beams are symmetrically arranged in two cones, with four beams (labeled S1, S2, S4, and N4) in the outer cone with a half-angle of 3.7° relative to the symmetric axis and the other four beams (labeled N1, N2, N3, and S3) in the inner cone with a half-angle of 2.4°. The aperture of each beam is 36×36 cm^2, and the focal length is 12 m. With each beam in the octad being individually tunable, through, for example, continuous-phase plates (CPP), spectral dispersion (SSD), polarization smoothing (PS), and multi-color mode, Shenguang Octopus is expected to be an excellent platform for LPI investigation.

In the shots reported in this paper, the target was a gold cylindrical hohlraum, 2.5 mm in diameter and 5.0 mm in length, filled with 0.6 atm neopentane (C_5H_{12}) gas. One end of the cylinder was closed and the other was covered by 400 nm thick polyimide film. CPPs were used to form a spot about 700 μm in diameter at the laser entrance hole (LEH). High-frequency (20 GHz) SSD was turned off, while low-frequency (2 GHz) SSD was routinely applied to each beam to protect the optics. Polarizations were set in the same direction. The designed incident laser power and pulse shape of all beams were the same (see the inset of Fig. 1), consisting of a 0.5 ns pre-pulse, a 0.5 ns through pulse, and a 3 ns square main pulse, with total energy 12 kJ, resulting in an overlapped intensity of about 1×10^{15} W/cm^2. In the single-color experiments, all eight beams were operated at 3ω ($\lambda_0 = 351$ nm, $\Delta\lambda = 0$ nm), termed the "1color" mode, whereas in the two-color experiments, the octad was operated in the "2color+" ($\Delta\lambda = +0.15$ nm, inner 351.15 nm, outer 350.85 nm) or "2color−" ($\Delta\lambda = -0.15$ nm, inner 350.85 nm, outer 351.15 nm) modes.

SBS and SRS backscattered light returning directly through the beamlines was measured using full aperture backscatter station (FABS) diagnostics. Backscattered light outside the focusing lenses was measured by a specially designed scatter plate, a near-backscattering imager (NBI). Each beam was diagnosed independently. Data from the FABS and NBI systems were absolutely calibrated to measure the SBS and SRS energies. The angular distribution of SBS light was obtained by combining the energy-normalized images from FABS and NBI, as shown in Fig. 2. The total time-averaged reflectivities of backward-scattered light at a level of 15% were measured, and were found to be dominated by SBS in spectrum and by FABS in space. The SRS reflectivity was at a level

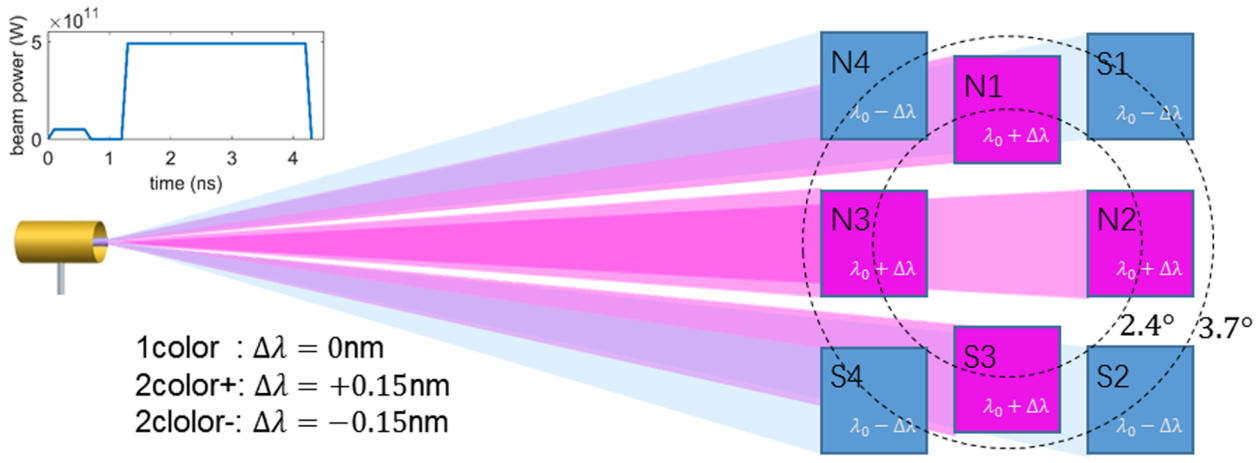

FIG. 1. Schematic representation of the octad LPI experiment on the Shenguang Octopus facility. The top left inset shows the incident power of each beam.

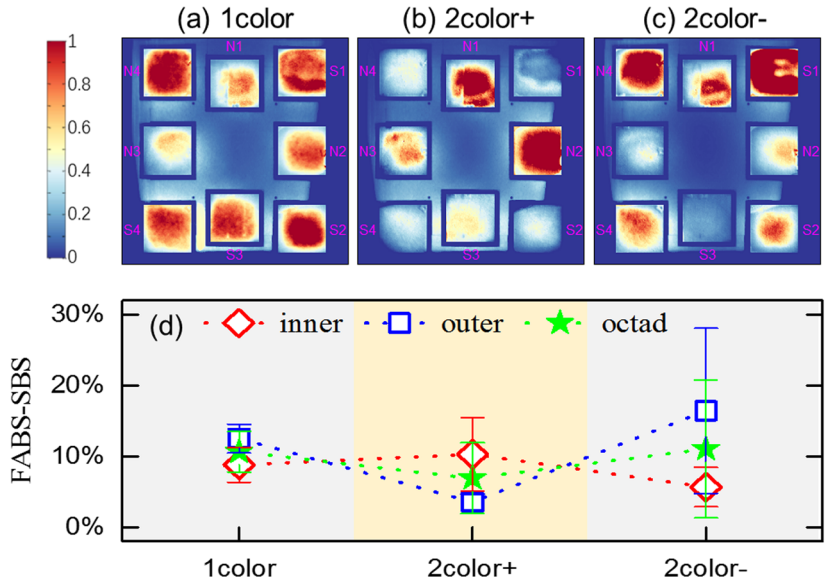

FIG. 2. (a)–(c) Measured angular distributions of SBS light for 1color, 2color+, and 2color− modes, respectively. (d) Statistics of measured FABS-SBS energy fraction. The red diamonds correspond to inner-cone averaging, the blue squares outer-cone averaging and the green stars octad averaging.

of <2%, and typical values of SBS reflectivities from FABS were at least five times those from the NBI. Multiple-beam collective SBS that shared a common scattered light along the symmetry axis was not observed. The discussion and analysis in this paper focus on the FABS-SBS. Figure 2(d) summarizes the FABS-SBS energy fractions of shots in the 1color, 2color+, and 2color− modes.

By tracing the rays under a pseudo-3D plasma condition obtained by rotating the 2D radiation hydrodynamic simulation results using the LARED-Integration code,[25] the steady-state linear LPI analysis provides a SBS spectrum that shows good consistency with measurements, confirming that the strong damping approximation is valid and SBS grows mainly in a convective manner in the first 1–2 mm of plasma near the LEH. The SBS spectrum does not show any significant signal of gold. SBS originating from the ablated Au plasma is no longer amplified in the filled gas, but is collisionally damped to the extent that it vanishes, since there is a mismatch in the spectrum of the convective SBS gain at the interface. Inside the region where a steep electron density gradient and a plasma flow are generated by ablation of the cover film, a millimeter-thick nearly homogeneous C_5H_{12} plasma is present, as can be seen in Fig. 3, which shows a typical plasma condition at t = 1.8 ns, 0.5 ns after the arrival of the main pulse. During the main pulse, the electron density n_e evolves to $(0.05–0.02)n_c$ within the region outlined by the dashed rectangle in Fig. 3 (here, $n_c = 9.05 \times 10^{21}$ cm^{-3} is the critical density for the 351 nm pump beams), the electron and ion temperatures are T_e = 1.6–1.1 keV and T_i = 0.60–0.55 keV, and $k\lambda_{De}$ = 0.5–0.7, where k is the IAW wavenumber and λ_{De} is the Debye length. SBS seeds coming from deeper in the C_5H_{12} plasma are convectively amplified here. Furthermore, according to the prediction of linear theory, a single beam of the experimental intensity $\sim 1.3 \times 10^{14}$ W/cm^2 is below its threshold and cannot excite convective SBS of ~10% energy fraction. To obtain convective SBS of >1% energy fraction, an incident beam with intensity greater than 5×10^{14} W/cm^2 is required. However, the total time-averaged octad SBS reflectivity is 11% for the 1color mode. This implies that the octad SBS is enhanced by the collective mechanism. The averaged SBS of the outer and inner cones are 12% and 9%, respectively, for the 1color mode. The outer cone SBS backscattering is slightly increases. One reason for this is that compared with the rays of the inner cone, those of the outer cone experience a plasma condition with higher n_e and lower T_e owing to the radial nonuniformity.

Interestingly, when two-color lasers are used, no matter whether they are inner or outer, the beams with longer incident wavelength are subject to a higher SBS gain. For the 2color+ mode, the averaged FABS-SBS of the outer and inner cones are 4% and 10%, respectively, while for the 2color− mode, the corresponding percentages are 16% and 6%. An intuitive explanation is that CBET may have occurred. Two light waves drive a transverse IAW resonantly, and energy is transferred from the shorter-wavelength beam to the longer-wavelength one. To estimate the CBET between inner beam and outer beam, for clarity we choose one ray near the outside of the laser path to investigate, as indicated in Fig. 3, and employ a steady-state model describing inverse bremsstrahlung absorption (IBA) and CBET coupling of two crossing laser beams. Many nonlinear saturation mechanisms are not taken account into this model, and the resonant CBET maybe overestimated; for details, see the Appendix. Figure 4(a) shows the coupling coefficient Γ_{CBET} as a function of wavelength shift $\Delta\lambda = \lambda_2 - \lambda_1$. The resonance peak location on axis $\Delta\lambda$ is determined by the plasma parameters and the largest angle between the inner and outer beams, ϕ (here, $\phi = 5.4^\circ$), and is Doppler-shifted by the plasma flow $\mathbf{u}_r \cdot \mathbf{k}_{\mathrm{iaw}}$, where $\mathbf{u}_r$ is the radial flow velocity and $\mathbf{k}_{\mathrm{iaw}}$ is the IAW vector. At the positive peak of Γ_{CBET}, energy is resonantly transferred from beam 1 to beam 2. Figure 4(b) show the relative energy gain of beam 2

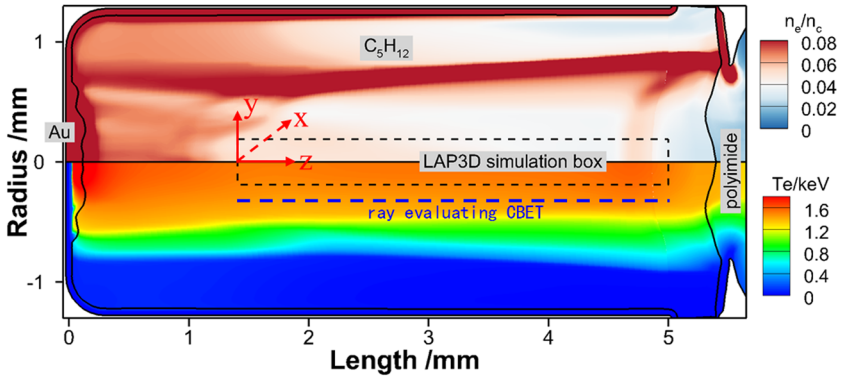

FIG. 3. Electron density n_e (in units of n_c) and electron temperature T_e (in keV) at t = 1.8 ns from the LARED-Integration code. The black solid lines indicate material boundaries, the black dashed rectangle indicates the LAP3D simulation box, and the blue dashed line indicate the ray where the CBET is evaluated in Fig. 4.

as a function of $\Delta\lambda$. The inset shows the geometric matching relationship between the three wave vectors. Two beams of intensity 1.3×10^{14} W/cm^2 are incident from the right boundary of Fig. 4(a). Without CBET, only taking IBA into account, the intensity of beam 2, I_2^{IBA}, is reduced to 60% when it reaches the left boundary. The relative energy gain of beam 2 is defined as $(I_2^{\mathrm{IBA,CBET}} - I_2^{\mathrm{IBA}})/I_2^{\mathrm{IBA}}$ at the left boundary, where $I_2^{\mathrm{IBA,CBET}}$ is the intensity of beam 2 considering both CBET and IBA. Figure 4(b) show that the wavelength separation required for resonant CBET is about 0.03 nm, one order of magnitude smaller than the wavelength separation of 0.3 nm in the experiment.

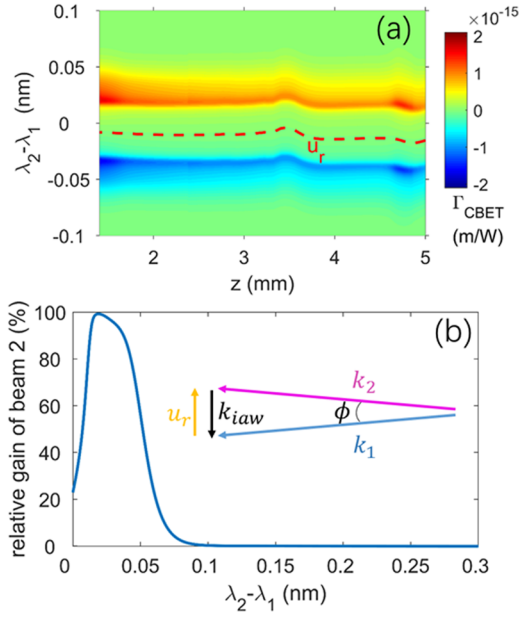

FIG. 4. (a) Coupling coefficient Γ_{CBET} along the ray indicated in Fig. 3 as a function of the wavelength shift $\Delta\lambda = \lambda_2 - \lambda_1$. (b) Relative energy gain of beam 2 as a function of $\Delta\lambda$.

Furthermore, the experimental results are symmetrical under interchange of the wavelengths of the inner and outer beams, indicating that the radial velocity of the plasma does not affect the three-wave matching condition for CBET. Therefore, it is necessary to seek other physical explanations beyond CBET. Figure 4(b) also indicates that there is net energy transfer from inner cone to outer cone when $\Delta\lambda = 0$.[26] This is another reason why the outer cone SBS is greater than that of the inner cone in the 1color mode.

Note in Fig. 2(d), the error bars of the longer-wavelength beams are greater than those of the shorter-wavelength beams. For the 2color− mode, the FABS-SBS of S1 is unexpectedly as high as 33%. The envelope of the temporal evolution of each beam's FABS-SBS power has been recorded by both a photon tube and an optical streak camera, and, together with its energy, the FABS-SBS power evolution has been obtained. The data show that the peak of S1 instantaneous FABS-SBS is achieved at almost 100% of beam power. Accounting for the NBI, at its peak, the instantaneous S1 SBS power exceeds the injected laser power, which is clear evidence that collective SBS occurs and part of the S1 SBS is pumped by other beams. This indicates that although in principle the two-color scheme is capable of suppressing SBS, a new risk may arise in the octad configuration, leading to a SBS burst, which could re-enter the beam line and possibly damage optical apparatus.[27]

III. 3D NUMERICAL RESULTS

A laser–plasma interaction code LAP3D has been developed that solves coupled wave–wave equations and includes absorption, refraction, diffraction, filamentation, SBS, SRS, and hydrodynamic evolution.[28] In the present work, only SBS is considered in LAP3D. As shown in Fig. 3, the simulation box is $0.36 \times 0.36 \times 3.6$ mm^3 in the x, y, z directions, discretized to $512 \times 512 \times 1024$ grid points, with the z axis along the symmetry axis of the target. 3D plasma conditions are obtained by rotating the 2D radiation hydrodynamic simulation result. Here, the plasma state at t = 1.8 ns is used for three cases. The electron density and temperature are $n_e \approx 0.04 n_c$ and $T_e \approx 1.5$ keV. The incident lasers are superpositions of eight beams after CPP smoothing, with SSD turned off, and polarization in the same direction. For the 1color, 2color+, and 2color− modes,

the octad total SBS energy fractions are 44.7%, 35.7%, and 29.8%, respectively. The simulation results are about three times the experimental results. In the experiment, the SBS duration time was less than 2 ns, and the instantaneous reflectivities were larger than the whole-time averaged results. This result shows that two-color light can suppress SBS. The angular distribution of SBS light at the lens is obtained by performing a 2D (x–y plane) Fourier transform of the backward SBS light. The time-integrated angular distributions of SBS light are shown in Figs. 5 (a)–5(c). The ratios of the FABS-SBS between the inner cone and outer cone, SBS_{inner}/SBS_{outer}, are 1.1, 2.8, and 0.48, respectively, for the three cases, while the experimental results are 0.75, 2.7, and 0.40, respectively, and so the results of simulation and experiment are qualitatively consistent. Although there are some discrepancies in reflectivity between experiment and simulation, the longer-wavelength beams have higher SBS reflectivity, demonstrating that the simulation has provided insight into the physics.

A simple model that considers each pair of beams in the octad sharing a common IAW is helpful for understanding the two-color effect. As shown in Fig. 6, it is assumed that two overlapping

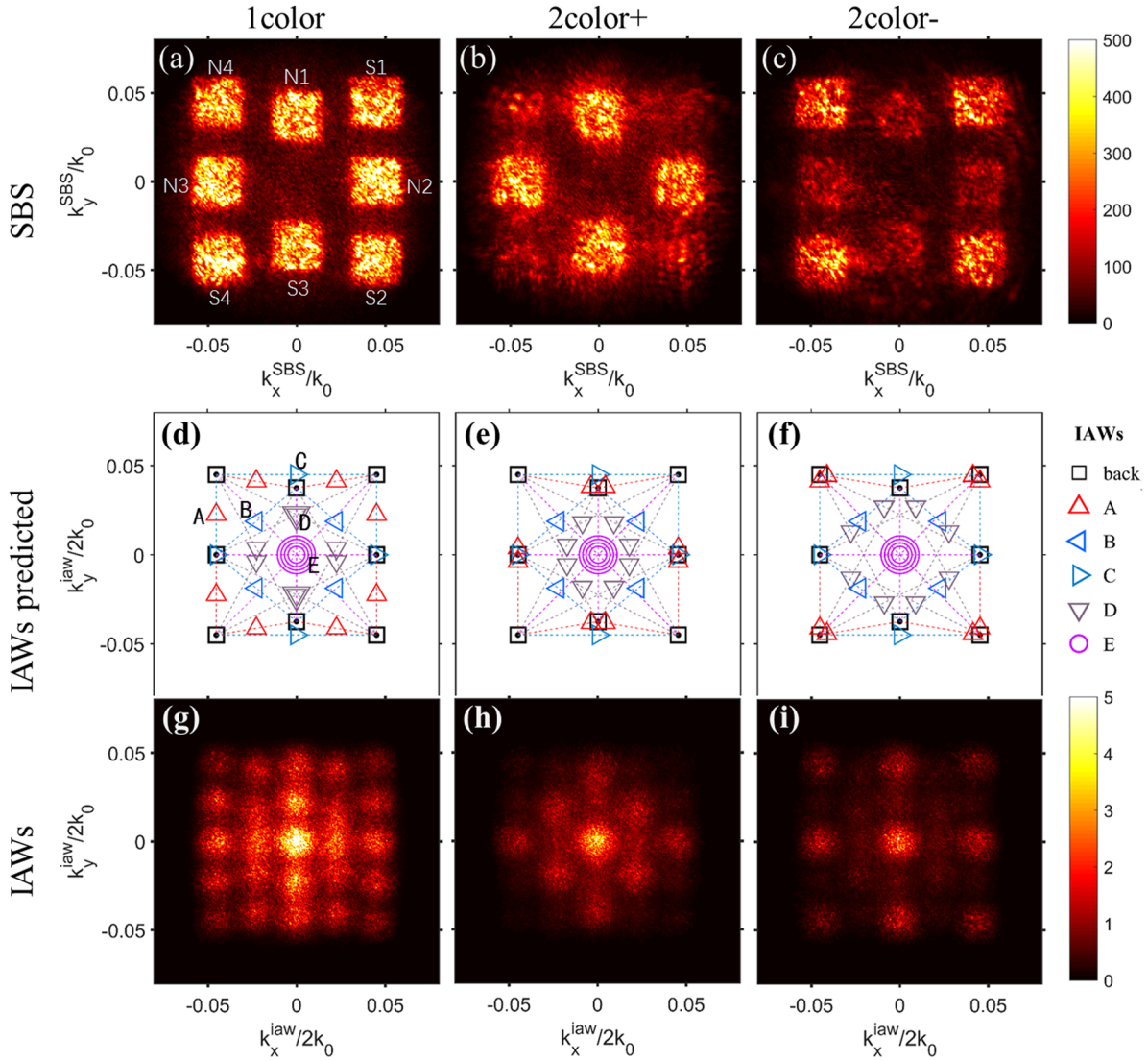

FIG. 5. (a)–(c) Time-integrated angular distributions of SBS intensity obtained by LAP3D simulation, with the same linear color map used for all. (d)–(f) Angular distributions of common IAWs according to the theoretical prediction. The squares denote the backscattering IAWs of each beam. The circles denote all possible $C_8^2 = 28$ IAWs shared by each pair of beams linked by a dashed line. (g)–(i) Time-integrated angular distributions of IAWs intensity obtained by LAP3D simulation, with the same linear color map used for all. (a), (d), and (g) are for the 1color mode, (b), (e), and (h) for the 2color+ mode, and (c), (f), and (i) for the 2color− mode. $k_0 = 2\pi/\lambda_0$ is the light wavenumber in vacuum.

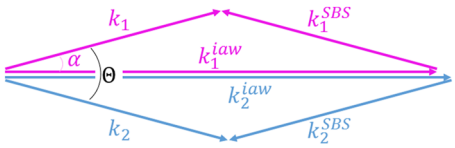

FIG. 6. Sketch map of wave vector matching triangles when two SBS process share one IAW.

incident lights (with wave vectors k_1 and k_2) with angle Θ between them excite SBS processes, sharing their IAWs with wave vectors k_1^{IAW} and k_2^{IAW} in the same direction (indicated by the angle α). k_1^{SBS} and k_2^{SBS} are the wave vectors of the scattered light. Assuming that laser k_1 has the longer wavelength ($\lambda_2 < \lambda_1$), that δ is the normalized wavelength shift [$\lambda_2 = \lambda_1(1-\delta)$ and $k_2 = k_1(1+\delta)$, with $\delta \ll 1$], and that Θ and α are small angles ($\Theta, \alpha \ll 1$), the normalized detuning between the two IAWs $\Delta\tilde{k}^{\mathrm{IAW}} \equiv \left(k_2^{\mathrm{IAW}} - k_1^{\mathrm{IAW}}\right)/2k_1$ is approximately $\delta + \alpha^2/2 - (\Theta - \alpha)^2/2$, where α and Θ are in radians. When $\Delta\tilde{k}^{\mathrm{IAW}} = 0$, i.e.,

$$\alpha = \Theta/2 - \delta/\Theta, \tag{1}$$

a perfect matching condition is satisfied, the five waves are coupled together, and the SBS will enhance each other. Here, the dimensionless parameter δ/Θ is related to the direction of the shared IAW. It indicates the existence of a competitive mechanism between the geometrical angle and the wavelength shift. If the two wavelengths are equal, then the shared IAW lies on the symmetry axis, $\alpha = \Theta/2$. In the octad, the angle between nearest beams is about $\Theta \approx 2.4°$. If the wavelength separation is 0.3 nm, then $\alpha \approx 0$, and the common IAW is nearly parallel to k_1, the direction of the longer-wavelength beam. In this case, the common IAW is superimposed on the backscattered IAW of beam k_1 and enhances its backscattering. It should be noted in Fig. 6 that the direction of the scattered light can be ray-retracing,[29] but this phenomenon does not affect the above relation. The SBS is mainly ray-retracing in the simulations, and some weak signals in other directions have also been observed in the 2color− case.

Using Eq. (1), all $C_8^2 = 28$ possible IAWs shared by each pair of beams in the octad are plotted in Figs. 5(d)–5(f). There are eight "A-type" IAWs excited by beams N4–N3, N4–N1, etc., four "B-type" IAWs excited by beams N1–N3, N1–N2, etc., four "C-type" IAWs excited by beams N4–S1, N4–S4, etc., eight "D-type" IAWs excited by beams N4–N2, S1–N3, etc., and four "E-type" IAWs excited by beams N2–N3, S1–S4, etc. The overlapping of D-type IAWs indicates that there each IAW is excited by four beams, namely, N4, S1, N2, and N3. Similarly, the four IAWs labeled as E-type are actually two IAWs excited by four beams of the inner or outer cone. The time-integrated angular distribution of IAW intensity obtained from LAP3D simulation in Fig. 5(g) perfectly represents the prediction in Fig. 5(d). When a two-color laser configuration is used, as shown in Figs. 5(e) and 5(f), the IAWs as a whole are weakened, leading to a suppression of octad SBS reflectivity. The A-type IAWs move toward beams of longer wavelength, making the IAWs of backscattering more stronger. For example, in Fig. 5(e), two A-type and one C-type IAW gather around N3, and in Fig. 5(f), two A-type IAWs gather around N4. In the 2color+ mode, the detuning between the IAW on the z-axis shared by the inner cone and the IAW shared by the outer cone is smaller than that in the 2color− mode, while both comparable to the bandwidth of the SBS resonance. Therefore, the simulated total SBS of the 2color+ mode is slightly stronger than that of the 2color− mode.

The laser property of each beam imprints a marked individuality on its FABS-SBS pattern, as shown in Fig. 2. In the two-color experiments, the fluctuation of beam SBS within the longer-wavelength cone is amplified compared with that within the shorter-wavelength cone, as is its cone-averaged SBS. In the LAP3D simulation, the discrepancy of laser properties between simulation and experiment is responsible for the absence of any representation of overbalance of beam SBS within a single cone.

IV. CONCLUSION

LPI experiments have been carried out on the Shenguang Octopus facility using multiple beams arranged symmetrically into two cones with competitive wavelength shift $\delta = \Delta\lambda/\lambda$ and geometrical angle Θ. Long-scale-length plasmas have been generated by illuminating a C_5H_{12}-filled gold cylindrical hohlraum. LAP3D simulations have successfully reproduced the SBS pattern and the relative reflectivity. The angular distributions of collectively driven IAWs are recomposed owing to a wavelength shift between the two cones, resulting in a cone (wavelength)-dependent enhancement of SBS reflectivity. The simulations of the effect of wavelength shift on SBS agree with the experimental data. This demonstrates that the detuning resulting from the geometrical angle can be retrieved by the wavelength shift, and vice versa. It has also been shown that the use of multi-color lasers to suppress LPI may give rise to a new risk that collective SBS resonance might be enhanced at a specific solid angle, and this possibility should be carefully considered. The findings of this study validate the physical modeling capabilities of the LAP3D code, qualifying it as an essential tool for studying LPI in complex laser configurations and subsequently for the design of future ICF experiments.

ACKNOWLEDGMENTS

This work is supported by the Natural Science Foundation of China (Grant Nos. 11975059, 12005021, and 11875241).

AUTHOR DECLARATIONS

Conflict of Interest

The authors have no conflicts to disclose.

Author Contributions

Q.W. and Z.L. contributed equally to this work. Q.W. was scientist for this experiment and performed simulations. Z.L. was lead experimentalist on the experiment and perfomed post-shot studies.

Qiang Wang: Conceptualization (lead); Formal analysis (lead); Software (equal); Writing – original draft (lead). **Zhichao Li**: Conceptualization (equal); Data curation (equal); Formal analysis (equal);

Software (equal); Writing – original draft (lead). **Zhanjun Liu**: Conceptualization (equal); Formal analysis (equal); Software (equal). **Tao Gong**: Data curation (equal); Formal analysis (equal). **Wenshuai Zhang**: Formal analysis (equal). **Tao Xu**: Data curation (equal). **Bin Li**: Formal analysis (equal). **Ping Li**: Data curation (equal). **Xin Li**: Software (equal). **Chunyang Zheng**: Formal analysis (equal). **Lihua Cao**: Formal analysis (equal). **Xincheng Liu**: Data curation (equal). **Kaiqiang Pan**: Data curation (equal). **Hang Zhao**: Data curation (equal). **Yonggang Liu**: Data curation (equal). **Bo Deng**: Data curation (equal). **Lifei Hou**: Data curation (equal). **Yingjie Li**: Data curation (equal). **Xiangming Liu**: Data curation (equal). **Yulong Li**: Data curation (equal). **Xiaoshi Peng**: Data curation (equal). **Zanyang Guan**: Data curation (equal). **Qiangqiang Wang**: Data curation (equal). **Xingsen Che**: Data curation (equal). **Sanwei Li**: Data curation (equal). **Qiang Yin**: Data curation (equal). **Wei Zhang**: Data curation (equal). **Liqiong Xia**: Data curation (equal). **Peng Wang**: Data curation (equal). **Xiaohua Jiang**: Data curation (equal). **Liang Guo**: Data curation (equal). **Qi Li**: Data curation (equal). **Minqing He**: Formal analysis (equal). **Liang Hao**: Formal analysis (equal). **Hongbo Cai**: Formal analysis (equal). **Wudi Zheng**: Formal analysis (equal). **Shiyang Zou**: Supervision (equal). **Dong Yang**: Data curation (equal). **Feng Wang**: Project administration (equal). **Jiamin Yang**: Project administration (equal). **Baohan Zhang**: Project administration (equal). **Yongkun Ding**: Project administration (equal). **Xiantu He**: Supervision (equal).

DATA AVAILABILITY

The data that support the findings of this study are available from the corresponding author upon reasonable request.

APPENDIX: EVALUATION OF CBET

Considering IBA and CBET, the evolution of the intensity of two crossing laser beams can be expressed as

$$\partial_s I_1 = -\frac{\nu_{ei}\omega_{pe}^2}{\omega_1 k_1 c^2} I_1 - \frac{\omega_1}{\omega_2}\Gamma_{\mathrm{CBET}} I_1 I_2,$$

$$\partial_s I_2 = -\frac{\nu_{ei}\omega_{pe}^2}{\omega_2 k_2 c^2} I_2 + \Gamma_{\mathrm{CBET}} I_1 I_2,$$

where

$$\Gamma_{\mathrm{CBET}} = \frac{gKk_{\mathrm{IAW}}^2}{k_1 k_2 \omega_1}, \qquad g = \frac{e^2}{2\epsilon_0 m_e^2 c^4},$$

$$K = \mathrm{Im}\left[\frac{\chi_e(1+\chi_i)}{1+\chi_i+\chi_e}\right],$$

$$k_{\mathrm{IAW}} = \sqrt{k_1^2 + k_2^2 - 2k_1 k_2 \cos\phi}.$$

Here, ω_{pe} and ν_{ei} are the electron plasma frequency and electron–ion collision frequency, χ_e and χ_i are the linear kinetic collisionless susceptibilities of Maxwellian electrons and ions, and m_e, e, and c are the electron mass, electron charge, and speed of light. Note that this evaluation is carried out along a specific ray. For a complete estimation of CBET between an inner beam and an outer beam in an octad, the averaged angle ϕ is smaller, the averaged ray path is shorter, and the projection of the radial flow velocity $\mathbf{u}_r$ on the IAW vector $\mathbf{k}_{\mathrm{IAW}}$ is smaller. There will be no essential change, however, to the conclusions that in the two-color case, the 0.3 nm separation is far away from the CBET resonance and that in the one-color case, a radial plasma flow can induce CBET from inner beams to outer beams.

REFERENCES

[1] J. D. Lindl, P. Amendt, R. L. Berger, S. G. Glendinning, S. H. Glenzer, S. W. Haan, R. L. Kauffman, O. L. Landen, and L. J. Suter, "The physics basis for ignition using indirect-drive targets on the National Ignition Facility," Phys. Plasmas **11**, 339 (2004).

[2] X. T. He, J. W. Li, Z. F. Fan, L. F. Wang, J. Liu, K. Lan, J. F. Wu, and W. H. Ye, "A hybrid-drive nonisobaric-ignition scheme for inertial confinement fusion," Phys. Plasmas **23**, 082706 (2016).

[3] K. Lan, J. Liu, Z. Li, X. Xie, W. Huo, Y. Chen, G. Ren, C. Zheng, D. Yang, S. Li, Z. Yang, L. Guo, S. Li, M. Zhang, X. Han, C. Zhai, L. Hou, Y. Li, K. Deng, Z. Yuan, X. Zhan, F. Wang, G. Yuan, H. Zhang, B. Jiang, L. Huang, W. Zhang, K. Du, R. Zhao, P. Li, W. Wang, J. Su, X. Deng, D. Hu, W. Zhou, H. Jia, Y. Ding, W. Zheng, and X. He, "Progress in octahedral spherical hohlraum study," Matter Radiat. Extremes **1**, 8 (2016).

[4] W. L. Kruer, S. C. Wilks, B. B. Afeyan, and R. K. Kirkwood, "Energy transfer between crossing laser beams," Phys. Plasmas **3**, 382 (1996).

[5] P. Michel, L. Divol, E. A. Williams, S. Weber, C. A. Thomas, D. A. Callahan, S. W. Haan, J. D. Salmonson, S. Dixit, D. E. Hinkel, M. J. Edwards, B. J. MacGowan, J. D. Lindl, S. H. Glenzer, and L. J. Suter, "Tuning the implosion symmetry of ICF targets via controlled crossed-beam energy transfer," Phys. Rev. Lett. **102**, 025004 (2009).

[6] P. Michel, S. H. Glenzer, L. Divol, D. K. Bradley, D. Callahan, S. Dixit, S. Glenn, D. Hinkel, R. K. Kirkwood, J. L. Kline, W. L. Kruer, G. A. Kyrala, S. Le Pape, N. B. Meezan, R. Town, K. Widmann, E. A. Williams, B. J. MacGowan, J. Lindl, and L. J. Suter, "Symmetry tuning via controlled crossed-beam energy transfer on the National Ignition Facility," Phys. Plasmas **17**, 056305 (2010).

[7] J. F. Myatt, J. Zhang, R. W. Short, A. V. Maximov, W. Seka, D. H. Froula, D. H. Edgell, D. T. Michel, I. V. Igumenshchev, D. E. Hinkel, P. Michel, and J. D. Moody, "Multiple-beam laser–plasma interactions in inertial confinement fusion," Phys. Plasmas **21**, 055501 (2014).

[8] D. Turnbull, P. Michel, J. E. Ralph, L. Divol, J. S. Ross, L. F. Berzak Hopkins, A. L. Kritcher, D. E. Hinkel, and J. D. Moody, "Multibeam seeded Brillouin sidescatter in inertial confinement fusion experiments," Phys. Rev. Lett. **114**, 125001 (2015).

[9] R. K. Kirkwood, D. P. Turnbull, T. Chapman, S. C. Wilks, M. D. Rosen, R. A. London, L. A. Pickworth, W. H. Dunlop, J. D. Moody, D. J. Strozzi, P. A. Michel, L. Divol, O. L. Landen, B. J. MacGowan, B. M. Van Wonterghem, K. B. Fournier, and B. E. Blue, "Plasma-based beam combiner for very high fluence and energy," Nat. Phys. **14**, 80 (2018).

[10] P. Michel, L. Divol, D. Turnbull, and J. D. Moody, "Dynamic control of the polarization of intense laser beams via optical wave mixing in plasmas," Phys. Rev. Lett. **113**, 205001 (2014).

[11] W. Seka, H. A. Baldis, J. Fuchs, S. P. Regan, D. D. Meyerhofer, C. Stoeckl, B. Yaakobi, R. S. Craxton, and R. W. Short, "Multibeam stimulated Brillouin scattering from hot, solid-target plasmas," Phys. Rev. Lett. **89**, 175002 (2002).

[12] S. Depierreux, C. Neuville, C. Baccou, V. Tassin, M. Casanova, P.-E. Masson-Laborde, N. Borisenko, A. Orekhov, A. Colaitis, A. Debayle, G. Duchateau, A. Heron, S. Huller, P. Loiseau, P. Nicolaï, D. Pesme, C. Riconda, G. Tran, R. Bahr, J. Katz, C. Stoeckl, W. Seka, V. Tikhonchuk, and C. Labaune, "Experimental investigation of the collective Raman scattering of multiple laser beams in inhomogeneous plasmas," Phys. Rev. Lett. **117**, 235002 (2016).

[13] C. Neuville, V. Tassin, D. Pesme, M.-C. Monteil, P.-E. Masson-Laborde, C. Baccou, P. Fremerye, F. Philippe, P. Seytor, D. Teychenné, W. Seka, J. Katz, R. Bahr, and S. Depierreux, "Experimental evidence of the collective Brillouin scattering of multiple laser beams sharing acoustic waves," Phys. Rev. Lett. **116**, 235002 (2016).

[14] S. Depierreux, C. Neuville, V. Tassin, M.-C. Monteil, P.-E. Masson-Laborde, C. Baccou, P. Fremerye, F. Philippe, P. Seytor, D. Teychenné, J. Katz, R. Bahr, M. Casanova, N. Borisenko, L. Borisenko, A. Orekhov, A. Colaitis, A. Debayle,

G. Duchateau, A. Heron, S. Huller, P. Loiseau, P. Nicolai, C. Riconda, G. Tran, C. Stoeckl, W. Seka, V. Tikhonchuk, D. Pesme, and C. Labaune, "Experimental investigation of the collective stimulated Brillouin and Raman scattering of multiple laser beams in inertial confinement fusion experiments," Plasma Phys. Controlled Fusion **62**, 014024 (2020).

[15]P. Michel, L. Divol, E. L. Dewald, J. L. Milovich, M. Hohenberger, O. S. Jones, L. B. Hopkins, R. L. Berger, W. L. Kruer, and J. D. Moody, "Multibeam stimulated Raman scattering in inertial confinement fusion conditions," Phys. Rev. Lett. **115**, 055003 (2015).

[16]D. F. DuBois, B. Bezzerides, and H. A. Rose, "Collective parametric instabilities of many overlapping laser beams with finite bandwidth," Phys. Fluids B **4**, 241 (1992).

[17]J. J. Thomson and J. I. Karush, "Effects of finite-bandwidth driver on the parametric instability," Phys. Fluids **17**, 1608 (1974).

[18]J. J. Thomson, "Finite-bandwidth effects on the parametric instability in an inhomogeneous plasma," Nucl. Fusion **15**, 237 (1975).

[19]S. P. Obenschain, N. C. Luhmann, Jr., and P. T. Greiling, "Effects of finite-bandwidth driver pumps on the parametric-decay instability," Phys. Rev. Lett. **36**, 1309 (1976).

[20]V. J. Harper-Slaboszewicz, K. Mizuno, T. Idehara, and J. S. De Groot, "Finite bandwidth drive effect on the parametric decay instability near the lower hybrid frequency," Phys. Fluids B **2**, 2525 (1990).

[21]P. N. Guzdar, C. S. Liu, and R. H. Lehmberg, "The effect of bandwidth on the convective Raman instability in inhomogeneous plasmas," Phys. Fluids B **3**, 2882 (1991).

[22]R. K. Follett, J. G. Shaw, J. F. Myatt, H. Wen, D. H. Froula, and J. P. Palastro, "Thresholds of absolute two-plasmon-decay and stimulated Raman scattering instabilities driven by multiple broadband lasers," Phys. Plasmas **28**, 032103 (2021).

[23]Z. Wanguo, Z. Xiaomin, W. Xiaofeng, J. Feng, S. Zhan, Z. Kuixin, Y. Xiaodong, J. Xiaodong, S. Jingqin, Z. Hai, L. Mingzhong, W. Jianjun, H. Dongxia, H. Shaobo, X. Yong, P. Zhitao, F. Bin, G. Liangfu, L. Xiaoqun, Z. Qihua, Y. Haiwu, Y. Yong, F. Dianyuan, and Z. Weiyan, "Status of the SG-III solid-state laser facility," J. Phys.: Conf. Ser. **112**, 032009 (2008).

[24]W. Zheng, X. Wei, Q. Zhu, F. Jing, D. Hu, X. Yuan, W. Dai, W. Zhou, F. Wang, D. Xu, X. Xie, B. Feng, Z. Peng, L. Guo, Y. Chen, X. Zhang, L. Liu, D. Lin, Z. Dang, Y. Xiang, R. Zhang, F. Wang, H. Jia, and X. Deng, "Laser performance upgrade for precise ICF experiment in SG-III laser facility," Matter Radiat. Extremes **2**, 243 (2017).

[25]P. Song, C. Zhai, S. Li, Y. Heng, J. Qi, X. Hang, R. Yang, J. Cheng, Q. Zeng, X. Hu, S. Wang, Y. Shi, W. Zheng, P. Gu, S. Zou, X. Li, Y. Zhao, H. Zhang, A. Zhang, H. An, J. Li, W. Pei, and S. Zhu, "LARED-Integration code for numerical simulation of the whole process of the indirect-drive laser inertial confinement fusion," High Power Laser Part. Beams **27**, 032007 (2015).

[26]K. B. Wharton, R. K. Kirkwood, S. H. Glenzer, K. G. Estabrook, B. B. Afeyan, B. I. Cohen, J. D. Moody, and C. Joshi, "Observation of energy transfer between identical-frequency laser beams in a flowing plasma," Phys. Rev. Lett. **81**, 2248 (1998).

[27]T. Chapman, P. Michel, J.-M. G. Di Nicola, R. L. Berger, P. K. Whitman, J. D. Moody, K. R. Manes, M. L. Spaeth, M. A. Belyaev, C. A. Thomas, and B. J. MacGowan, "Investigation and modeling of optics damage in high-power laser systems caused by light backscattered in plasma at the target," J. Appl. Phys. **125**, 033101 (2019).

[28]Z. J. Liu, Q. Wang, W. S. Zhang, B. Li, P. Li, L. H. Cao, W. G. Zheng, X. Li, and J. W. Li, "Suppression of stimulated Brillouin scattering by multi-color alternating-polarization bundle light in inertial confinement fusion," Phys. Plasmas **30**, 032703 (2023).

[29]Z. J. Liu, Z. Li, Q. Wang, T. Gong, W. Zhang, T. Xu, B. Li, P. Li, X. Li, L. Cao, C. Zheng, X. Liu, K. Pan, H. Zhao, Y. Liu, B. Deng, L. Hou, Y. Li, X. Liu, Y. Li, X. Peng, Z. Guan, Q. Wang, X. Che, S. Li, Q. Yin, W. Zhang, L. Xia, P. Wang, X. Jiang, L. Guo, L. Qi, H. Liang, H. Cai, W. Zheng, S. Zou, Y. Dong, F. Wang, J. Yang, B. Zhang, Y. Ding, and X. T. He, "Ray retracing of stimulated Brillouin scattering in the smoothed bundle-beam laser low density plasma interaction experiments" (unpublished).